Featured in Physics

Potential of Attosecond Coherent Diffractive Imaging

Arjun Rana,[1,†] Jianhua Zhang,[1,2,†] Minh Pham,[3] Andrew Yuan,[1] Yuan Hung Lo,[1,4]
Huaidong Jiang,[2] Stanley J. Osher,[3] and Jianwei Miao[1,*]

[1]*Department of Physics & Astronomy, STROBE NSF Science & Technology Center and California NanoSystems Institute, University of California, Los Angeles, California 90095, USA*
[2]*School of Physical Science and Technology, ShanghaiTech University, Shanghai 201210, China*
[3]*Department of Mathematics, University of California, Los Angeles, California 90095, USA*
[4]*Department of Bioengineering, University of California Los Angeles, California 90095, USA*

(Received 26 March 2020; revised 28 June 2020; accepted 20 July 2020; published 19 August 2020)

Attosecond science has been transforming our understanding of electron dynamics in atoms, molecules, and solids. However, to date almost all of the attoscience experiments have been based on spectroscopic measurements because attosecond pulses have intrinsically very broad spectra due to the uncertainty principle and are incompatible with conventional imaging systems. Here we report an important advance towards achieving attosecond coherent diffractive imaging. Using simulated attosecond pulses, we simultaneously reconstruct the spectrum, 17 probes, and 17 spectral images of extended objects from a set of ptychographic diffraction patterns. We further confirm the principle and feasibility of this method by successfully performing a ptychographic coherent diffractive imaging experiment using a light-emitting diode with a broad spectrum. We believe this work clears the way to an unexplored domain of attosecond imaging science, which could have a far-reaching impact across different disciplines.

DOI: 10.1103/PhysRevLett.125.086101

The first demonstration of attosecond pulses in 2001 opened a new window to probe electron dynamics in atoms and molecules with unprecedented time resolution [1–9]. With the continuing decrease of the temporal pulse duration and the increase of the photon energy range to the x-ray regime [10–14], the potential applications of attoscience could be even broader. However, attoscience experiments have been mostly limited to spectroscopic techniques due to the broad spectrum of the attosecond source [3–5]. For an attosecond pulse, its energy bandwidth (ΔE) and temporal pulse duration (Δt) are fundamentally set by the uncertainty principle ($\Delta E \Delta t \geq \hbar/2$). For example, the recent experimental demonstration of 53 asec soft x-ray pulses reaches the carbon K-absorption edge (284 eV) with $\Delta E/E \approx 100\%$ [13]. Such broad spectrum pulses cause severe chromatic aberration for any lens-based imaging systems. Chromatic aberration, first discovered by Newton more than 300 years ago [15], is a failure of a lens to focus all colors to the same focal spot due to the change of the refractive index of the lens with the wavelength of light. A classical method to overcome chromatic aberration is the use of achromatic lenses [16]. But this method does not work for the full spectrum of electromagnetic radiation. For example, design and manufacture of achromatic lenses are extremely challenging in the x-ray regime, where lens design is difficult even in the monochromatic case [17]. Here we introduce a novel method based on coherent diffractive imaging (CDI), which can not only eliminate chromatic aberration associated with optical lenses, but also take advantage of the broad spectrum to simultaneously reconstruct the spectrum, probes, and images at 17 different wavelengths.

CDI is a lensless imaging or computational microscopy method, where the diffraction patterns of an object are first measured and then directly phased to obtain high-resolution images [18]. Since the first experimental demonstration in 1999 [19], various forms of CDI such as plane-wave CDI, ptychography, and Bragg CDI have been developed and applied to a broad range of samples in the physical and biological sciences using synchrotron radiation, x-ray free electron lasers, high harmonic generation, optical lasers, and electrons [18–31]. With advanced computational algorithms, broadband CDI has also been developed to deal with the low temporal coherence of the illumination source [32–36]. Ptychography, a powerful scanning CDI method, is particularly suitable for broadband imaging, which collects a series of diffraction patterns by scanning a spatially confined probe across an extended sample [22,31]. By partially overlapping the probe between adjacent scan positions, advanced algorithms can be used to reconstruct both the probe and the complex exit wave of the sample [23]. More recently, multimode and multiplex ptychographic methods have been developed to deal with broadband data [37–42]. In this Letter, we make an important advance to merge CDI with attosecond science, allowing the simultaneous reconstruction of the spectrum, probes, and images at multiple wavelengths.

 © 2020 American Physical Society

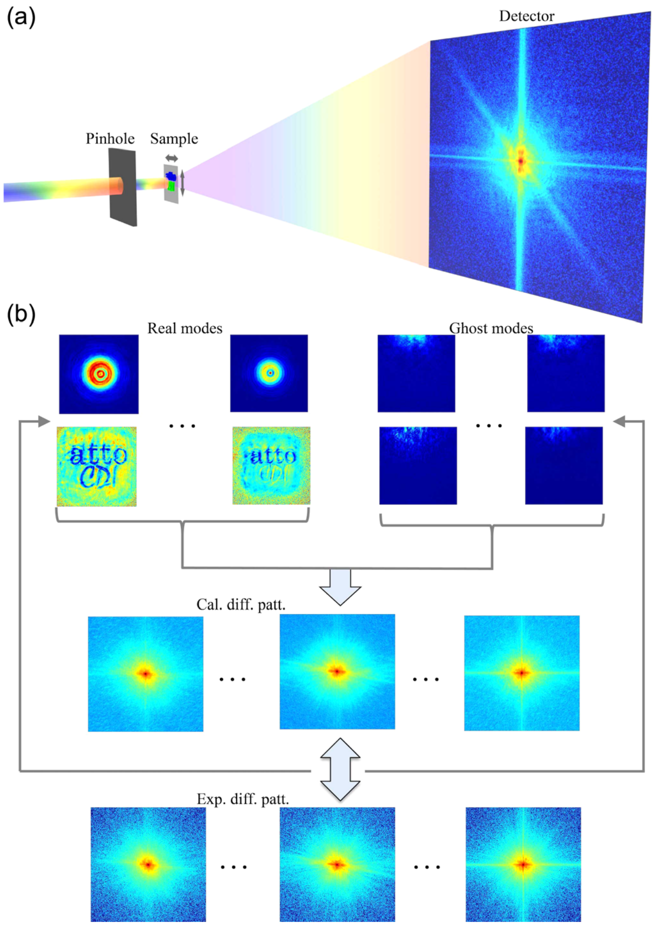

FIG. 1. Schematic of the broadband CDI data acquisition and SPIRE algorithm. (a) A probe with a very broad spectrum is defined by a pinhole and scanned across a sample. At each scan position, a diffraction pattern is recorded by a detector. (b) SPIRE iterates between real and reciprocal space. In real space, the exit wave of the real and ghost modes at different wavelengths is obtained by multiplying probes by the object functions of the sample. In reciprocal space, the calculated diffraction patterns at different scan positions are compared with the corresponding experimental diffraction patterns, which is used to update the real and ghost modes of the next iteration. A detailed description of SPIRE is provided in the Supplemental Material [44].

For attosecond light with a broad bandwidth, its diffraction pattern is composed of an incoherent sum of diffracted intensity from all wavelengths, producing a blurred pattern [Fig. 1(a)]. Phase retrieval of such blurred diffraction patterns is a challenging process as they are mixed with both coherent and incoherent scattering. Here we develop an advanced algorithm, called Spectrum, Probe, and Image REconstruction (SPIRE), to simultaneously reconstruct the spectrum, probes, and spectral images at multiple wavelengths. SPIRE requires the collection of a set of diffraction patterns by performing a 2D scan of a confined probe across a sample, where the probe at each scan position is overlapped with its adjacent ones [Fig. 1(a)]. To meet the criterion that the number of the equations of measured intensity points is more than the number of unknown variables of the sample [43], a large overlap between adjacent scan positions is needed. The algorithm then iterates between real and reciprocal space [Fig. 1(b)]. In real space, we introduce the concept of real and ghost modes, where the real modes reconstruct the spectrum, probes, and spectral images, and the ghost modes accommodate unwanted information such as errors and noise (Supplemental Material [44]). The exit wave of the real and ghost modes at different wavelengths is obtained by multiplying probes by the object functions of the sample. Taking the Fourier transform of the exit wave generates the diffracted wave of real and ghost modes. An updated diffracted wave is obtained by constraining it to the diffraction patterns. Applying the inverse Fourier transform to the diffracted wave produces a new exit wave, which is used to create the next-iteration probes and object functions of the real and ghost modes. In each iteration, we also enforce the probe replacement constraint to the real modes. The best probe is identified among all the wavelengths and is propagated back to construct the probes of other wavelengths. By incorporating the real, ghost modes, and probe replacement, SPIRE enables us to simultaneously reconstruct the spectrum, probes, and spectral images from a very broadband illumination. The algorithm is robust as it is not sensitive to the initial input and converges after several hundreds of iterations.

To validate the SPIRE algorithm, we first performed numerical simulations using attosecond pulses with a spectrum ranging from 4.1 to 12.4 nm [13]. The probe was confined by a 3-μm-diameter pinhole that was placed 100 μm upstream of the sample and Fresnel propagated to the sample plane. Two samples were used in the simulations. The first is a resolution pattern, composed of 200-nm-thick aluminum structure with bar widths ranging from 30 nm to 1.2 μm. The second sample is a letter pattern with “atto” made of 200-nm-thick aluminum and “CDI” of 200-nm-thick boron. Boron was chosen because its K-absorption edge (6.6 nm) is within the simulated spectrum, providing a contrast difference to assess the reconstruction quality of the spectrum and spectral images. Each sample was scanned in a randomly perturbed 2D raster grid scheme with a 94% overlap between adjacent scan positions. The resolution pattern dataset consists of 1456 scan points and the letter pattern dataset consists of 676 scan points. A flux of 1×10^7 photons per scan position was used in the simulation and Poisson noise was added to the diffraction intensity. Each diffraction pattern was collected by a detector positioned 10 cm downstream of the sample to satisfy the oversampling requirement for all wavelengths [43]. The quantum efficiency of the detector as a function of the spectrum was taken into account in each diffraction pattern. Figures 2(a) and 2(b) show a representative diffraction pattern from the resolution and letter pattern, respectively. The most

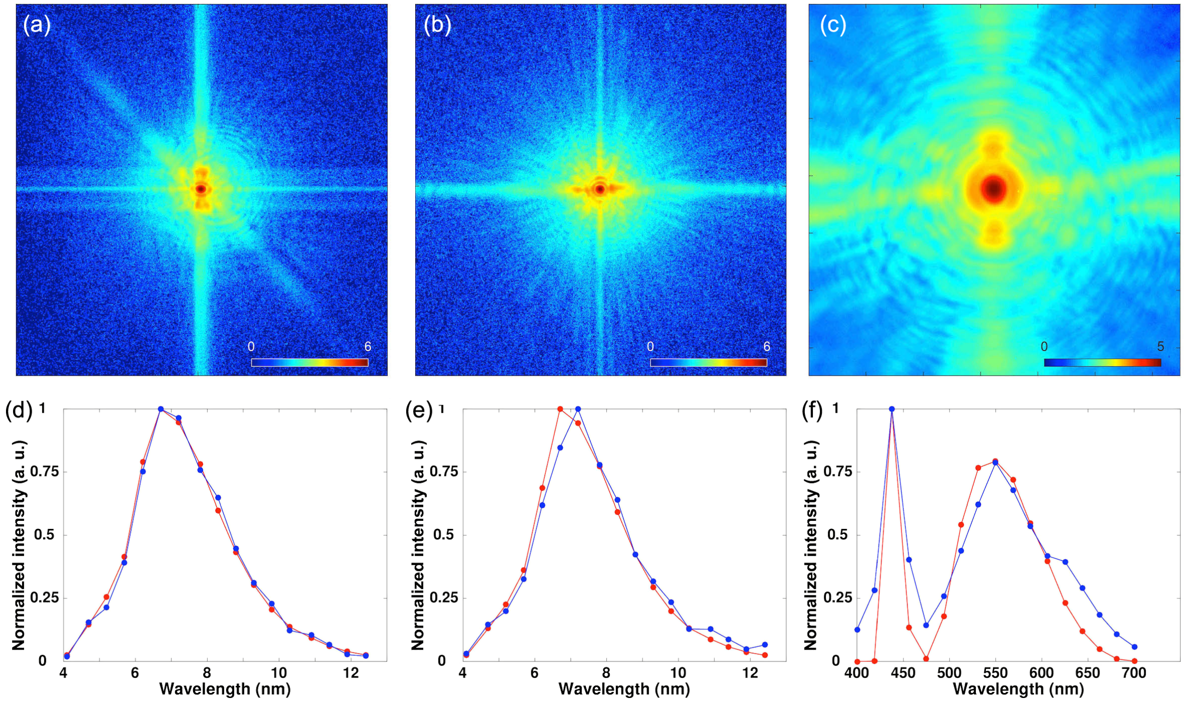

FIG. 2. Representative diffraction patterns and reconstructed spectra by SPIRE. (a) and (b) Representative diffraction patterns measured from a resolution and letter pattern, respectively, using simulated attosecond pulses. (c) Representative diffraction pattern of a test pattern using an LED. (d)–(f) Reconstructed spectra (in blue) of the resolution and letter pattern with simulated attosecond pulses and of the test pattern with the LED, respectively, where the true spectra are in red. The true spectrum of the LED in (f) was measured by a spectrometer.

noticeable feature of these broadband diffraction patterns is the absence of strong speckles that are presented in monochromatic diffraction patterns.

From the diffraction patterns, we used the SPIRE algorithm to reconstruct the spectrum, probes, and spectral images. All reconstructions consist of two runs of 250 iterations each. In the first run, the initial guesses of the probes and spectral images were binary masks and random arrays, respectively. The second run was initialized with new random arrays of the images while retaining the reconstructed probes from the first run. In the second run, only the images were allowed to update while the probes are fixed. In all reconstructions, we chose 17 probes and 17 spectral images that span the simulated spectrum in equal wavelength intervals. The number of probes and spectral images was heuristically chosen in a manner to reconstruct the spectrum with high accuracy while also minimizing the crosstalk between adjacent images. Figures 2(d)–2(e) show the reconstructed spectra (blue) of the resolution and letter pattern, which are in good agreement with the true ones (red). In comparison, a state-of-the-art broadband algorithm known as ptychographic information multiplexing (PIM) [38] failed to reconstruct the spectra in both cases (Supplemental Material, Fig. S1 [44]). Figure 3 shows the SPIRE reconstruction of the probes and spectral images of the resolution pattern at three

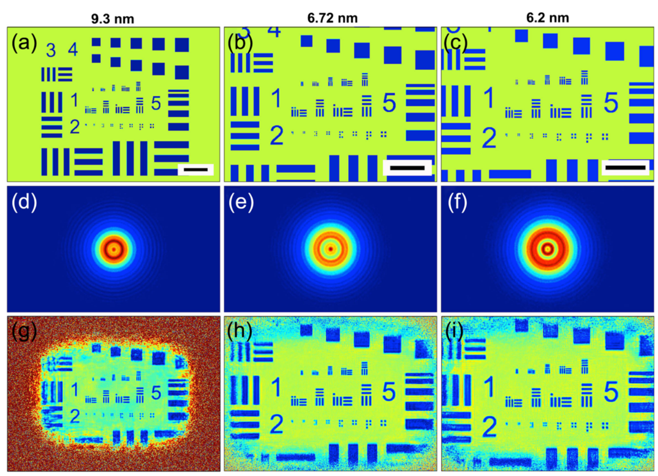

FIG. 3. Probe and spectral image reconstructions of a resolution pattern with simulated attosecond pulses. (a)–(c) The structure of the resolution pattern at 9.3, 6.72, and 6.2 nm, respectively. (d)–(i) Three representative probes and spectral images at different wavelengths reconstructed by SPIRE, respectively, where the spatial resolution is increased with the decrease of the wavelength. The full 17 probes and 17 spectral images are shown in Supplemental Material, Figs. S2(a) and S3(a) [44], respectively. Scale bars, 2 μm.

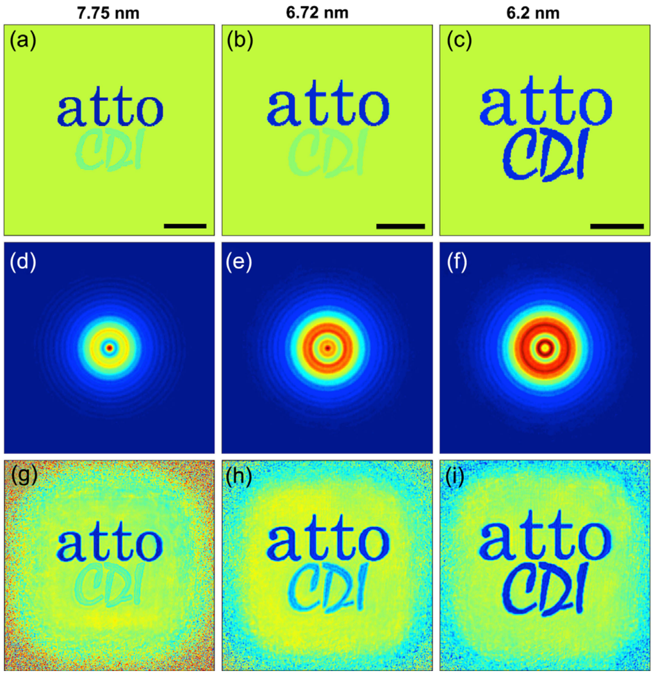

FIG. 4. Probe and spectral image reconstructions of a letter pattern with simulated attosecond pulses. (a)–(c) Absorption contrast images of the letter pattern at 7.75, 6.72, and 6.2 nm, respectively, where the *K* edge of boron is at 6.6 nm. (d)–(i) Three representative probes and spectral images at different wavelengths reconstructed by SPIRE, respectively, where the image contrast of the "CDI" letters changes across the absorption edge. The full 17 probes and 17 spectral images are shown in the Supplemental Material, Figs. S4(a) and S5(a) [44], respectively. Scale bars, 2 μm.

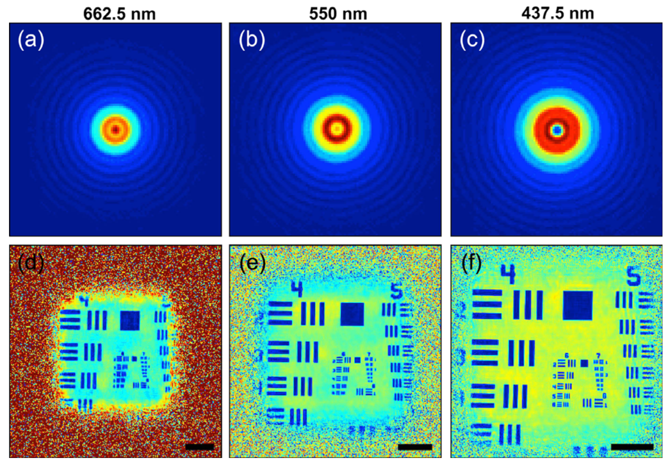

FIG. 5. Probe and spectral image reconstructions of a test pattern from broadband LED diffraction patterns. (a)–(f) Three representative probes and spectral images reconstructed by SPIRE at 662.5, 550, and 437.5 nm, respectively. The full 17 probes and 17 spectral images are shown in Supplemental Material, Fig. S8 [44]. Scale bars, 200 μm.

representative wavelengths (9.3, 6.72, 6.2 nm), in which the spatial resolution is increased with the decrease of the wavelength. The full reconstructions of 17 probes and 17 spectral images are shown in the Supplemental Material [44], Figs. S2(a) and S3(a), respectively. SPIRE faithfully reconstructed all the probes and spectral images except the first and last image due to the low incident flux at these two wavelengths [Fig S3(a), frame 1 and 17]. Figure 4 and Figs. S4(a) and S5(a), and video S1 in the Supplemental Material [44] show the reconstructed probes and spectral images of the letter pattern. While the absorption of aluminum is relatively flat across the spectrum, the *K* edge of boron at 6.6 nm causes a jump in the absorption contrast of the "CDI" letters (Fig. 4). In comparison, PIM failed to reconstruct several probes and spectral images of both the resolution and letter patterns [Supplemental Material [44], Figs. S2(b), S3(b), 4S(b), and S5(b)]. To account for the spectral instability of attosecond pulses, we conducted another simulation with a shot-to-shot spectral fluctuation of 10%. With all the other parameters kept the same, SPIRE successfully reconstructed the average spectrum, probes, and spectral images at 17 different wavelengths (Supplemental Material [44], Figs. S6 and S7).

Next, we performed a broadband light-emitting diode (LED) experiment to validate the method. A collimated white LED was used to illuminate a test pattern with a 200 μm pinhole placed approximately 6 mm upstream of the sample to confine the probe. A CCD camera from Princeton Instruments was placed 26 cm downstream of the sample to collect diffraction patterns while fulfilling the oversampling requirement for all wavelengths of the LED [43]. A field of view approximately 600×600 μm was scanned using a 2D raster grid consisting of 950 points with a 94% overlap between adjacent probe positions. A small random offset was applied to the scan positions to avoid gridding artifacts in the reconstructions. Three exposures of different duration were collected at each scan position and merged to improve the dynamic range of the diffraction patterns. Diffraction patterns were cropped to be square and binned by a factor of 2 in each dimension to increase the signal-to-noise ratio and reduce the computation time. After two runs of 250 iterations each, we reconstructed the spectrum, 17 probes, and 17 spectral images from the diffraction patterns. The reconstructed spectrum agrees with that measured by a spectrometer [Fig. 2(f)]. Figure 5 shows three representative probes and spectral images at 662.5, 550, and 437.5 nm. All 17 probes and images are shown in the Supplemental Material [44], Fig. S8. The successful reconstruction of the spectrum, probes, and spectral images from the experimental diffraction patterns further corroborated the feasibility of the method.

In conclusion, we have developed a powerful algorithm (SPIRE) by incorporating new constraints—real, ghost modes, and probe replacement. Our simulation and experimental results demonstrate that SPIRE can simultaneously reconstruct the spectrum, probes, and spectral images at

17 wavelengths from very broadband light sources with $\Delta E/E \approx 100\%$, which (to our knowledge) cannot currently be accomplished by any other broadband CDI algorithms [32–42]. Looking forward, we anticipate that SPIRE is in principle applicable to both coherent photon and electron sources with broad spectra, such as synchrotron radiation pink beams and HHG, allowing chemically specific imaging without the need of monochromatic optics. By avoiding the use of focusing optics, the spatial resolution of this method is limited only by the spatial frequency of the diffracted intensity. Furthermore, by harnessing all the flux from a broadband light source, this method can significantly reduce the data acquisition time in performing spectroptychography experiments, whereas the conventional method requires serial repetition of ptychographic scans as a function of the energy. Finally, this work potentially unifies two important fields—attosecond science and CDI—into a single frame. As the spectrum of the current state-of-the-art attosecond sources extends to the x-ray regime [13,14], the ability to simultaneously reconstruct the spectrum, probes, and images at multiple wavelengths could find application ranging from visualizing attosecond electron dynamics to imaging materials and biological samples at the nanometer scale with attosecond x-ray pulses.

We thank Z. Chang, P. B. Corkum, M. M. Murnane, H. C. Kapteyn, Y. Wu, X. Ren, and J. Li for stimulating discussions. This work was primarily supported by STROBE: A National Science Foundation Science & Technology Center under Grant No. DMR 1548924. We also acknowledge partial support by the US Department of Energy, Office of Science, Basic Energy Sciences, Division of Materials Sciences and Engineering under Award No. DE-SC0010378.

*Corresponding author.
miao@physics.ucla.edu
†These authors contributed equally to this work.

[1] P. M. Paul, E. S. Toma, P. Breger, G. Mullot, F. Augé, Ph. Balcou, H. G. Muller, and P. Agostini, Science **292**, 1689 (2001).
[2] M. Hentschel, R. Kienberger, C. Spielmann, G. A. Reider, N. Milosevic, T. Brabec, P. Corkum, U. Heinzmann, M. Drescher, and F. Krausz, Nature (London) **414**, 509 (2001).
[3] F. Krausz and M. Ivanov, Rev. Mod. Phys. **81**, 163 (2009).
[4] P. B. Corkum and F. Krausz, Nat. Phys. **3**, 381 (2007).
[5] P. Agostini and L. F. DiMauro, Rep. Prog. Phys. **67**, 1563 (2004).
[6] A. Baltuška *et al.*, Nature (London) **421**, 611 (2003).
[7] J. Itatani, J. Levesque, D. Zeidler, H. Niikura, H. Pépin, J. C. Kieffer, P. B. Corkum, and D. M. Villeneuve, Nature (London) **432**, 867 (2004).
[8] A. L. Cavalieri *et al.*, Nature (London) **449**, 1029 (2007).
[9] G. Sansone *et al.*, Nature (London) **465**, 763 (2010).
[10] G. Sansone *et al.*, Science **314**, 443 (2006).
[11] H. Kapteyn, O. Cohen, I. Christov, and M. Murnane, Science **317**, 775 (2007).
[12] T. Popmintchev *et al.*, Science **336**, 1287 (2012).
[13] J. Li, X. Ren *et al.*, Nat. Commun. **8**, 186 (2017).
[14] T. Gaumnitz, A. Jain, Y. Pertot, M. Huppert, I. Jordan, F. Ardana-Lamas, and H. J. Wörner, Opt. Express **25**, 27506 (2017).
[15] I. Newton, *Opticks* (Royal Society, London, 1704).
[16] M. Daumas, *Scientific Instruments of the Seventeenth and Eighteenth Centuries and their Makers* (Portman Books, London, 1989).
[17] W. Chao, B. D. Harteneck, J. A. Liddle, E. H. Anderson, and D. T. Attwood, Nature (London) **435**, 1210 (2005).
[18] J. Miao, T. Ishikawa, I. K. Robinson, and M. Murnane, Science **348**, 530 (2015).
[19] J. Miao, P. Charalambous, J. Kirz, and D. Sayre, Nature (London) **400**, 342 (1999).
[20] H. N. Chapman *et al.*, Nat. Phys. **2**, 839 (2006).
[21] K. J. Gaffney and H. N. Chapman, Science **316**, 1444 (2007).
[22] J. M. Rodenburg, A. C. Hurst, A. G. Cullis, B. R. Dobson, F. Pfeiffer, O. Bunk, C. David, K. Jefimovs, and I. Johnson, Phys. Rev. Lett. **98**, 034801 (2007).
[23] P. Thibault, M. Dierolf, A. Menzel, O. Bunk, C. David, and F. Pfeiffer, Science **321**, 379 (2008).
[24] Y. Nishino, Y. Takahashi, N. Imamoto, T. Ishikawa, and K. Maeshima, Phys. Rev. Lett. **102**, 018101 (2009).
[25] I. Robinson and R. Harder, Nat. Mater. **8**, 291 (2009).
[26] M. M. Seibert *et al.*, Nature (London) **470**, 78 (2011).
[27] G. Zheng, R. Horstmeyer, and C. Yang, Nat. Photonics **7**, 739 (2013).
[28] D. F. Gardner *et al.*, Nat. Photonics **11**, 259 (2017).
[29] M. Holler, M. Guizar-Sicairos, E. H. R. Tsai, R. Dinapoli, E. Müller, O. Bunk, J. Raabe, and G. Aeppli, Nature (London) **543**, 402 (2017).
[30] Y. Jiang, Z. Chen, Y. Han, P. Deb, H. Gao, S. Xie, P. Purohit, M. W. Tate, J. Park, S. M. Gruner, V. Elser, and D. A. Muller, Nature (London) **559**, 343 (2018).
[31] F. Pfeiffer, Nat. Photonics **12**, 9 (2018).
[32] L. W. Whitehead, G. J. Williams, H. M. Quiney, D. J. Vine, R. A. Dilanian, S. Flewett, K. A. Nugent, A. G. Peele, E. Balaur, and I. McNulty, Phys. Rev. Lett. **103**, 243902 (2009).
[33] B. Abbey *et al.*, Nat. Photonics **5**, 420 (2011).
[34] S. Witte, V. T. Tenner, D. W. Noom, and K. S. Eikema, Light Sci. Appl. **3**, e163 (2014).
[35] J. Huijts, S. Fernandez, D. Gauthier, M. Kholodtsova, A. Maghraoui, K. Medjoubi, A. Somogyi, W. Boutu, and H. Merdji, arXiv:1909.11345.
[36] J. Huijts, Ph.D. thesis, Université Paris-Saclay 2019, https://tel.archives-ouvertes.fr/tel-02183193/document.
[37] P. Thibault and A. Menzel, Nature (London) **494**, 68 (2013).
[38] D. J. Batey, D. Claus, and J. M. Rodenburg, Ultramicroscopy **138**, 13 (2014).
[39] B. Enders, M. Dierolf, P. Cloetens, M. Stockmar, F. Pfeiffer, and P. Thibault, Appl. Phys. Lett. **104**, 171104 (2014).
[40] B. Enders, Ph.D. Thesis, Technical University of Munich, Germany2016, https://pdfs.semanticscholar.org/7d86/c7625263394466ddbb442eebf75150d9b639.pdf.

[41] B. Zhang, D. F. Gardner, M. H. Seaberg, E. R. Shanblatt, C. L. Porter, R. Karl, C. A. Mancuso, H. C. Kapteyn, M. M. Murnane, and D. E. Adams, Opt. Express **24**, 18745 (2016).

[42] B. K. Chen, P. Sidorenko, O. Lahav, O. Peleg, and O. Cohen, Opt. Lett. **43**, 5379 (2018).

[43] J. Miao, D. Sayre, and H. N. Chapman, J. Opt. Soc. Am. A **15**, 1662 (1998).

[44] See Supplemental Material at http://link.aps.org/supplemental/10.1103/PhysRevLett.125.086101 for supplemental text and supplemental figures, which includes Ref. [45].

[45] A. M. Maiden and J. M. Rodenburg, Ultramicroscopy **109**, 1256 (2009).